CHEMICAL ENGINEERING TRANSACTIONS
VOL. 100, 2023
A publication of AIDIC
The Italian Association of Chemical Engineering
Online at www.cetjournal.it
Guest Editors: Sauro Pierucci, Flavio Manenti

ISBN 979-12-81206-03-8; **ISSN** 2283-9216
DOI: 10.3303/CET23100061

Bubble Column Reactors: the Variables Influencing the Mono-Dispersed Homogeneous Flow Regime

Nicolò Varallo, Giorgio Besagni*, Riccardo Mereu

Politecnico di Milano, Departmenet of Energy, Via Lambruschini 4, Milan 20156, Italy
giorgio.besagni@polimi.it

The fluid dynamics of large-diameter bubble columns explicates in six flow regimes emergin upon an increase in the gas flow rate and can be described and predicted via correct modelling of the flow regime transition coordinates. This study focuses on the transition between the mono-dispersed and poly-dispersed homogeneous flow regime and defines a statistical approach to determine the significative variables influencing the transition. The analysis is performed by coupling: (a) the Ordinary Least Squares method (OLS), to determine the relationship between the variables, (b) the Variance Inflation Factor (VIF), to check for multicollinearity issues, and (c) the Least Absolute Shrinkage and Selection Operator (LASSO), to select suitable variables. Subsequently, the Classification and Regression Tree (CART) approach has been applied to generate homogenous clusters of bubble columns in terms of flow regime transition.

1. Introduction

Two-phase bubble columns are multiphase reactors where a gas distributor disperses a gas phase into a continuous liquid phase in the form of dispersed bubbles.Bubble columns are widely used in many industrial applications since they offer several advantages, such as excellent heat and mass transfer between the phases, high durability and low operating and maintenance costs due to the absence of moving parts (Kantarci et al., 2005).The simplest bubble column configuration consists of a vertical vessel, in which the gas enters at the bottom through a gas sparger, and the liquid phase is supplied in the batch mode, or it may be co-current or counter-current to the rising bubbles (Figure 1).

2. Flow Regimes

In multiphase reactors, the flow regimes inform about the behavior of the dispersed phase and its interaction with the continuous phase. The fluid dynamics of large-diameter bubble columns explicates in six flow regimes and is interpreted by a function of two global fluid-dynamics parameters, the drift flux and the gas holdup. The analytical form of the function builds on five flow regime transition points (Figure 2) (more details in Besagni, 2021).

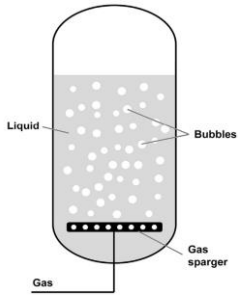

Figure 1: Bubble column reactor.

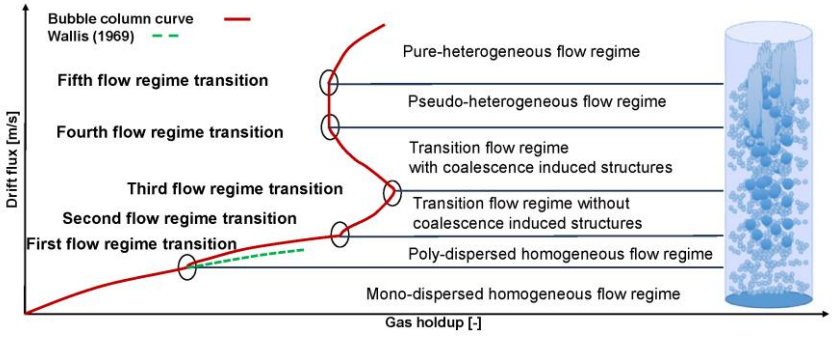

Figure 2: Bubble column characteristic curve (Besagni, 2021).

Paper Received: 1 March 2023; Revised: 21 March 2023; Accepted: 11 May 2023
Please cite this article as: Varallo N., Besagni G., Mereu R., 2023, Bubble Column Reactors: the Variables Influencing the Mono-dispersed Homogeneous Flow Regime, Chemical Engineering Transactions, 100, 361-366 DOI:10.3303/CET23100061

The drift flux is defined as the volumetric flux of either components relative to a surface moving at volumetric average velocity expressed as follow:

$$J_T = U_G(1-\varepsilon_G) \pm U_L\varepsilon_G \quad (1)$$

In Eq(1) ε_G is the gas holdup (defined as the volume of the dispersed phase divided by the total volume), U_G is the superficial gas velocity, and U_L is the superficial liquid velocity. The sign on the right-hand side depends on the operation mode of the bubble column: co-current mode (+) or counter-current mode (-); $U_L = 0$ in the batch mode.The six flow regimes, emerging upon an increase in the gas flow rate are: (1) mono-dispersed homogeneous flow regime, (2) poly-dispersed homogeneous flow regime, (3) transition flow regime without coalescence-induced structures, (4) transition flow regime with coalescence-induced structures, (5) pseudo-heterogeneous flow regime, and (6) pure-heterogeneous flow regime.
The transition between the mono-dispersed and poly-dispersed homogeneous flow regime can be detected by comparing the experimental drift flux values (J_T) with theoretical values (J_E) written in terms of bubble swarm velocity (v_b) (Wallis, 1969):

$$J_E = v_b(1-\varepsilon_G) \quad (2)$$

In Eq(2), the bubble swarm velocity (v_b) can be calculated with the following (Krishna et al., 1999):

$$v_b = u_\infty(1-\varepsilon_G)^{n-1} \quad (3)$$

Where n is fluid-dependent ($n \approx 2$ for water) and u_∞- the terminal velocity of an isolated bubble – should be fitted with the aid of experimental data in the determination of the flow regime transition point. In the mono-dispersed homogeneous $J_T = J_E$, and the transition to the poly-dispersed homogeneous flow regime occurs when:

$$J_E \neq J_T \quad (4)$$

3. The Statistical Analysis

3.1 Variables

As for the dependent variables Eq(4) has been applied to find the transition coordinate (i.e. transitional gas holdup, $\varepsilon_{G,trans}$, and transitional superficial gas velocity, $U_{G,trans}$) of several large-diameter bubble columns operating in batch and counter-current mode with different gas distributors, aspect ratio values and liquid phase properties (Table 1). Concerning the predictors, three main categories have been considered: geometrical characteristics of the column, operating conditions and liquid phase properties (Table 2).

3.2 Methods

Regression

The regression procedure (Figure 3) consists of five steps. In the first step, a dependent variable is selected out of $\varepsilon_{G,trans}$ and $U_{G,trans}$. In the second step, a class of predictors is selected out of the three groups listed in Section 3.1. In the third step, the regression procedure is applied to the selected dependent variable and the selected class of predictors (*"partial regression models"*). Subsequently, the above described steps (#1 to #3) are iterated until all the dependent variables have been considered and all the *"partial regression models"* have been obtained. In the fourth step the predictors found significant, after the regression procedure, are coupled and the regression analysis is performed again to obtain the *"aggregate regression model "*. Step#2 and step#3 are iterated until all the classes of predictors have been evaluated with respect to the depend variables and all the *"aggregate regression models"* have been obtained
The OLS – VIF – LASSO procedure applied at step#3 and step#4, is discussed in the following:

- **Phase#a.** A linear Ordinary Least Squares (OLS) is performed to relate the dependent variable with the selected class of predictors:

$$y_i = \beta_0 + \beta_1 x_{i1} + \beta_2 x_{i2} + \cdots + \beta_k x_{ik} + \varepsilon_i = \beta_0 + \sum_{j=1}^{w} \beta_j x_{ij} + \varepsilon_i \quad (5)$$

Where y_i is the selected dependent variable, x_{ij} is the j-predictor for the i-dependent variable out of w-predictors, β_0 is the constant term (intercept), β_j is the j-coefficient for the x_{ij} variable, ε_i is the error having null mean and constant variance.
The overall model fit is assessed based on the adjusted coefficient of determination (R^2_{adj}):

$$R^2_{adj} = 1 - \frac{SS_E/(n-k-1)}{SS_T/(n-1)} = 1 - \frac{(n-1)}{(n-k-1)}(1-R^2) \quad (6)$$

Table 1: Bubble column configurations analysed.

Reference	Liquid phase	D_c [m]	AR [-]	Sparger	d_0 [mm]	Operating condition
(Deckwer et al., 1974)	Water	0.20	1	Perforated plate	1	Open tube; batch
(Letzel et al., 1997)	Water	0.16	0.13	Perforated plate	0.5	Open tube; batch
(Ruzicka et al., 2001)	Water	0.29 – 0.40	0.34→4.14	Perforated plate	0.5	Open tube; batch
(Vandu et al., 2004)	Water	0.15 – 0.40	10.67	Perforated plate	0.5	Open tube; batch
(Chilekar et al., 2007)	Water	0.29	0.18	Perforated plate	0.5	Open tube; batch
(Ruzicka et al. 2008)	Water	0.15 – 0.38	2.86	Perforated plate	0.5	Open tube; batch
	$CaCl_2$ solution	0.14	2.86	Perforated plate	0.5	Open tube; batch
(Sal et al., 2013)	Water	0.33	1	Perforated plate	1	Open tube; batch
	Water	0.24	1→15	Perforated plate	0.5	Open tube; batch
	Water	0.24	1→15	Perforated plate	1	Open tube; batch
	Water	0.24	1→15	Needle	0.5	Open tube; batch
	Water	0.24	1→15	Spider	2→4	Open tube; batch
(Besagni, 2021)	Water	0.24	12.5	Pipe sparger	3	Open tube–annular gap; batch–counter-current
	NaCl solution	0.24	5 →10	Spider	2→4	Open tube; batch
	EtOH solution	0.24	5 →12.5	Spider	2→4	Open tube; batch
	MEG solution	0.24	5 →12.5	Spider	2→4	Open tube; batch

Table 2: Predictors used for the statistical analysis.

Geometrical characteristics	Operating conditions	Liquid phase properties
Column diameter (D_C)	Superficial liquid velocity (U_L)	Viscosity (μ)
Sparger hole diameter (d_0)	Presence of internals	Density (ρ)
Sparger type		Surface tension (σ)
Free area (FA)		
Aspect ratio (AR)		

Where SS_E is the sum of squares error minimization, SS_T is the sum of the total squares of the residuals, k is the number of independent variables and n is the number of observations.
Given the suspected issue of multicollinearity (i.e. correlation between the independent variables) the Variance Inflation Factor (VIF) is inspected for every β_j parameter:

$$VIF_j = \frac{1}{1-R_j^2} \quad (7)$$

If predictors are uncorrelated $VIF = 1$; if $VIF > 1$ possible correlations exist. A cut-off value (VIF_{MAX}) of 3.3 has been used in this study (Besagni and Borgarello , 2018) . In case of multicollinearity, the method proceeds towards phase#b, conversely, it proceeds towards phase#d.

- **Phase#b.** In the case of multicollinearity, LASSO is applied. LASSO is a variable shrinkage based on penalty, which selects relevant predictors by a constrained optimization problem, which results in the minimization of the following equation:

$$\sum_{i=1}^{n}\left(y_i - \beta_0 - \sum_{j=1}^{k}\beta_j x_{ij}\right)^2 + \lambda\sum_{j=1}^{k}|\beta_j| = SS_E + \lambda\sum_{j=1}^{k}|\beta_j| \quad (8)$$

In Eq(9), the first term is the sum of the squared residuals, whereas the second term is the sum of the regression coefficients, so that some of these latter shrink to zero and excluded from the analysis. $\lambda \geq 0$ is a tuning parameter controlling the amount of shrinkage. The λ value has been selected in order to obtain a cross-validation error within one standard deviation (λ_{SE}). Once the significant variables have been selected, OLS is repeated with the remaining variables; finally VIFs are inspected again: if multicollinearity has not been detected, the method is completed; conversely, the method proceeds to phase#c.

- **Phase#c.** A selection of predictors is accomplished by eliminating the least significant predictors one by one and, at each step, the changes in R^2_{adj} are monitored (a reduction of R^2_{adj} is considered acceptable if within 0.5 %) and the VIFs are evaluated (in this phase $VIF_{MAX} = 10$ (Besagni and Borgarello 2018)).

- **Phase#d.** A selection of the predictors is obtained through the recursive procedure described in *phase#c;* in this phase, a reduction of R^2_{adj} is considered acceptance if within 0.2 %).

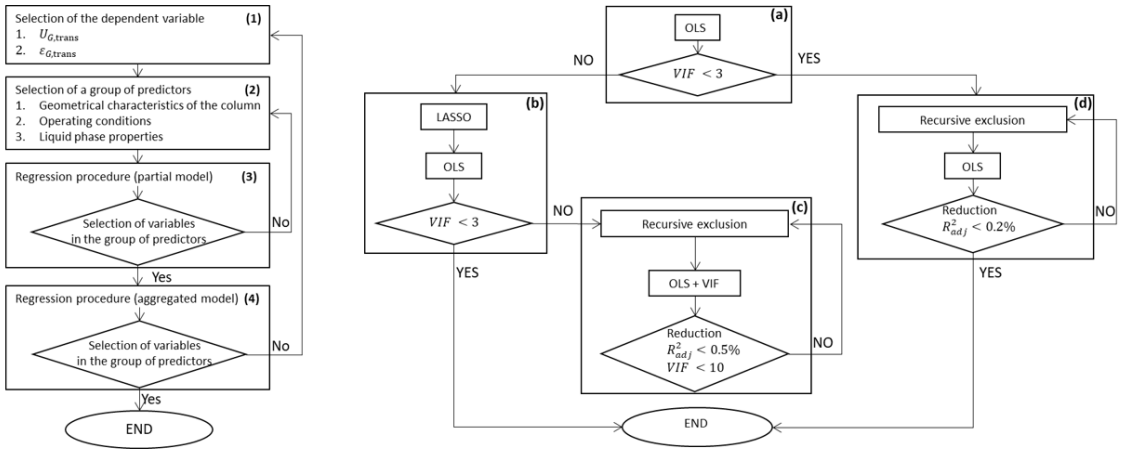

Figure 3: Statistical procedure (a) and OLS-VIF-LASSO procedure (b) overview.

Segmentation

The Classification and Regression Tree (CART) approach is based on a binary and recursive partitioning of the dataset and uses a flowchart-like tree structure to divide the entire dataset into homogeneous clusters. The splitting is based on the selection of the independent variable which allow the largest reduction in Eq(10):

$$SS_P - (SS_L + SS_R) \tag{9}$$

Where $SS_P = \sum(z - \bar{z})$ is the sum of the squares of the parent node and SS_L and SS_R are the sum of the squares of the left and right children nodes. The splitting is controlled by the complexity parameter (cp): at every split R^2_{CART} should increase of, at least, cp, where R^2_{CART} is defined as follows:

$$R^2_{CART} = 1 - \underbrace{\frac{\sum_{t\in\tilde{T}}\sum_{i\in\tilde{t}}[z_i - \bar{z}(t)]^2}{\sum_{i=1}^{n}[z_i - \bar{z}]^2}}_{relative\ error} \tag{10}$$

Where $\bar{z}$ is the predicted dependent variable, for the terminal node t, defined as the mean value of the dependent variable at that node; the sum at the numerator covers all the terminal nodes $t \in \tilde{T}$.

Implementation

The procedure was implemented in the open-source software R (release# 4.2.2).

4. Results

Coefficient of determination

Table 3 displays R^2_{adj} for the different regression models. The transition to the poly-dispersed homogeneous flow regime is influenced mainly by the geometrical characteristics of the column ($R^2_{adj,\varepsilon_{G,trans}} = 56.75\,\%$ and $R^2_{adj,U_{G,trans}} = 54.99\,\%$). The operating conditions variables mostly influence $U_{G,trans}$ ($R^2_{adj} = 26.68\,\%$) rather than $\varepsilon_{G,trans}$ ($R^2_{adj} = 8.34\,\%$). Concerning the liquid phase properties, they explain the 14.28 % of the $U_{G,trans}$ variance whereas they slightly influence $\varepsilon_{G,trans}$ ($R^2_{adj} = 2.94\,\%$). The *"aggregate regression models"* explain 60.63 % of $\varepsilon_{G,trans}$ and 64.65 % of $U_{G,trans}$.

Table 3: Coefficient of determination

	Class of predictors	Dependent variable	
		$\varepsilon_{G,trans}$	$U_{G,trans}$
"Partial regression models"	Geometrical characteristics	56.75 %	54.99 %
	Operating conditions	8.34 %	26.68 %
	Liquid phase properties	2.94 %	14.28 %
"Aggregate regression models"		60.63 %	64.65 %

Regression models and segmentation

The details of the *"aggregate regression models"* are displayed in Table 4 and Table 5. The first row displays the value of the intercept, β_0, whereas in the subsequent rows, the other coefficients, β_j, are listed. For every variable the following information were provided: value of the coefficients, standard error, *t*-test value, *p-value* (indicated by $Pr(>|t|)$), VIF value and level of significance. In all cases, the residuals were checked by the Quantile-Quantile plot inspection to determine if the data came from some theoretical distribution.

The information provided by the aggregate models highlights how an increment in the sparger hole diameter destabilizes the mono-dispersed homogeneous flow regime, causing a reduction of $\varepsilon_{G,trans}$ and $U_{G,trans}$. The same conclusion can be drawn for the aspect ratio since an increase in the aspect ratio reduces both $\varepsilon_{G,trans}$ and $U_{G,trans}$.

Table 4: Aggregate regression model for $\varepsilon_{G,trans}$.

	Coefficient	Std. error	*t*-value	$Pr(>\|t\|)$	VIF	Significance
Intercepts	0.26285	7.92E-03	33.209	<2E-16	-	***
Sparger holes diameter	-0.03324	4.07E-03	-8.167	2.72E-13	1.6	***
Aspect ratio	-0.00413	1.02E-03	-4.038	9.27E-05	1.6	***
Viscosity	-0.00506	1.37E-03	-3.693	3.28E-04	1	***

Table 5: Aggregate regression model for $U_{G,trans}$.

	Coefficient	Std. error	*t*-value	Pr(>|t|)	VIF	Significance
Intercepts	0.05179	1.40E-03	37.103	<2E-16	-	***
Sparger holes diameter	-0.00361	7.21E-04	-5.011	1.79E-06	1.7	***
Aspect ratio	-0.00096	1.80E-04	-5.361	3.82E-07	1.7	***
Superficial liquid velocity	0.10994	2.95E-02	3.731	2.87E-04	1.3	***
Viscosity	0.00111	2.36E-04	4.712	6.37E-06	1	***

Concerning the superficial liquid velocity an increment of $1\ m/s$ in its value (the sign is herein considered) leads to an increase in $U_{G,trans}$ of 10.99 % indicating that the counter current mode (i.e. negative value of superficial liquid velocity) destabilizes the mono-dispersed homogeneous flow regime.

The regression models does not clearly describe the effect of the viscosity: as the viscosity increases $\varepsilon_{G,trans}$ decreases but, at the same time, $U_{G,trans}$ increases and so a general conclusion cannot be reached.

The results of the CART approach are presented in Figure 4 and Figure 5. Considering $\varepsilon_{G,trans}$ regression tree (10 splits, 11 clusters), geometrical characteristics and fluid properties are used to split the dataset. The first, and most important, segmentation is based on the sparger hole diameter ($d_0 = 0.6\ mm$) differentiating between *"coarse sparger"* and *"fine sparger"*. The aspect ratio is the second important variable, followed by the liquid phase viscosity. Regarding $U_{G,trans}$ regression tree (9 splits, 10 clusters), the first segmentation is based on the aspect ratio value ($AR = 4.9$). The superficial liquid velocity splits the dataset only when columns with AR greater than 4.9 are considered since the dataset provides information on counter-current operation only for $AR \geq 5$.

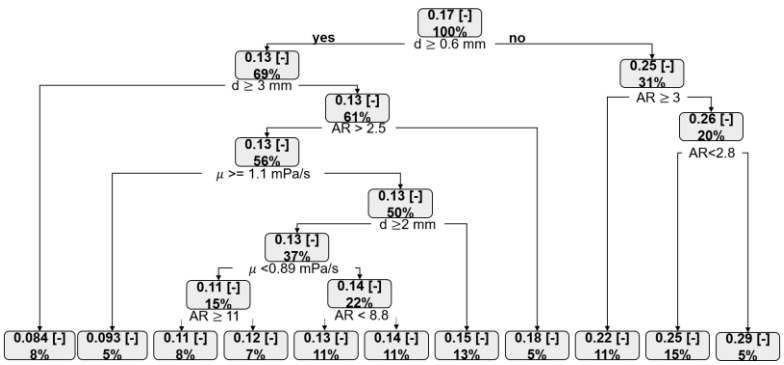

Figure 4: Bubble column segmentation, $\varepsilon_{G,trans}$

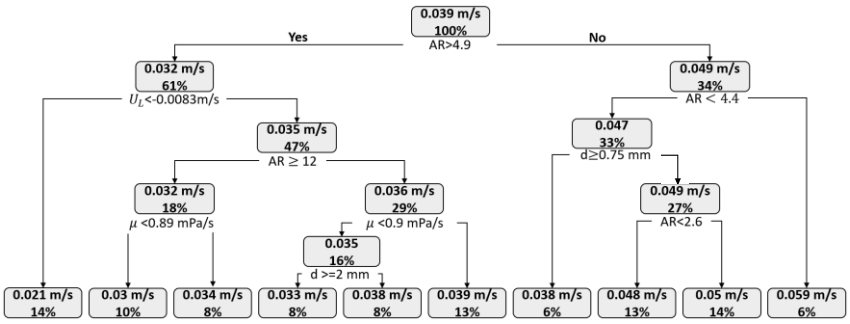

Figure 5: Bubble column segmentation, $U_{G,trans}$

5. Conclusion

This study proposes a statistical method to identify the predictors of the transition between the mono-dispersed and the poly-dispersed homogeneous flow regime. It was found that the geometrical characteristics of the column are significant in determining the flow regime transition ($R^2_{adj,\varepsilon_{G,trans}} = 56.75\ \%, R^2_{adj,U_{G,trans}} = 54.99\ \%$), followed by the operating conditions and liquid phase properties. In addition, the results of the CART method (provided as regression trees) make it straightforward to determine the transition point for a given bubble column and agree with those of the regression approach. The method proposed can be applied to the other flow regime transitions and future studies should extend the validity of the approach proposed by extending the present dataset. For example, column operating in co-current mode and with different pressures and temperatures should be considered.

References

Besagni G., Borgarello M., 2018, The determinants of residential energy expenditure in Italy, Energy, 165, pp. 369-386.

Besagni G., 2021, Bubble column fluid dynamics: A novel perspective for flow regimes and comprehensive experimental investigations, International Journal of Multiphase Flow, 135, p. 103510.

Chilekar V. P., Singh C., Van Der Schaaf J., Kuster B.F.M., Schouten J.C., 2007, A Gas hold-up model for slurry bubble columns, AIChE Journal, 53(7), pp. 1687–1702.

Deckwer W. D., Burckhart R., Zoll G., 1974, Mixing and mass transfer in tall bubble columns, Chemical Engineering Science, 29(11), pp. 2177–2188.

Kantarci N., Borak F., Ulgen K. O., 2005, Bubble Column Reactors, ChemInform, 40(7), pp. 2263-2283.

Krishna R., Ellenberger J., Maretto C., 1999, Flow regime transition in bubble columns, International Communications in Heat and Mass Transfer, 26 (4), pp 467-475.

Letzel H.M., Schouten J.C., Van Der Bleek C.M., 1997, Characterization of regimes and regime transitions in bubble columns by chaos analysis of pressure signals, Chemical Engineering Science, 52 (24), pp. 4447-4459.

Ruzicka M.C., Drahoš J., Fialová M., Thomas N.H., 2001, Effect of bubble column dimensions on flow regime transition, Chemical Engineering Science, 56 (21-22), pp. 6117-6124.

Ruzicka M.C., Vecer M. M., Orvalho S., Drahoš J., 2008,). Effect of surfactant on homogeneous regime stability in bubble column, Chemical Engineering Science, 63 (4), pp. 951-967.

Şal S., Gül Ö. F., Özdemir M., 2013, The effect of sparger geometry on gas holdup and regime transition points in a bubble column equipped with perforated plate spargers, Chemical Engineering and Processing: Process Intensification, 70, pp. 259-266.

Vandu C. O., Koop K., Krishna R., 2004, Large Bubble Sizes and Rise Velocities in a Bubble Column Slurry Reactor, Chemical Engineering & Technology, 27 (11), pp. 1195-1199.

Wallis G.B., One-dimensional two-phase flow, New York, McGraw-Hill.